THE JOURNAL OF PHYSICAL CHEMISTRY Letters

LETTER

pubs.acs.org/JPCL

Protofibrillar Assembly Toward the Formation of Amyloid Fibrils

Jesper Sørensen,[†] Xavier Periole,[‡] Katrine K. Skeby,[†] Siewert-J. Marrink,[‡] and Birgit Schiøtt*[,†]

[†]The Center for Insoluble Protein Structures (inSPIN) and the Interdisciplinary Nanoscience Center (iNANO), Department of Chemistry, Aarhus University, Langelandsgade 140, DK-8000 Aarhus C

[‡]Groningen Biomolecular Sciences and Biotechnology Institute and Zernike Institute for Advanced Materials, University of Groningen, Groningen, The Netherlands

Supporting Information

ABSTRACT: The formation and growth of amyloid fibrils was investigated using coarse-grained molecular dynamics simulations. In particular, we studied the assembly of amylin-(20−29) peptides, preassembled into protofibril fragments. The systems consisted of 27 protofibril fragments initially distributed onto a regular cubic grid with random orientation. Their association was followed on the μs time scale. At 300 K, it was observed that, while the assemblies formed are mainly disordered, there was an apparent preference for the fragments to associate such that an elongation of the structures predominates over their lateral extension. Increasing the temperature in the simulations resulted in an increase of the contact surfaces and allowed for rearrangement within the prefibrillar aggregates over longer time scales. The preferential elongation-like growth mechanism observed at 300 K was not persistent at higher temperatures indicative of a shift in growth pathway, congruent with experimental observations that changing growth conditions alters the morphology of the fibrils.

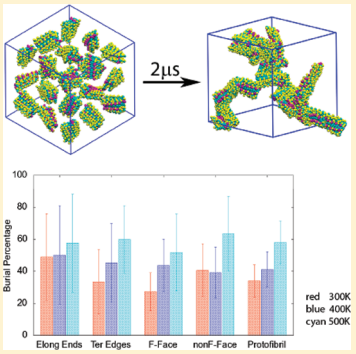

SECTION: Biophysical Chemistry

Amyloid fibrils are highly ordered protein aggregates sharing a cross-β spine structure, which consists of a pair of twisted β-sheets running parallel to the long axis of the fibril.[1,2] Assembly of peptides and proteins into amyloid fibrils and subsequent deposition of these fibrils in certain organs is associated with a variety of degenerative diseases.[3,4] For instance, in over 90% of patients with late-onset diabetes, amyloid deposits, mainly comprised of the human islet amyloid polypeptide (hIAPP), also known as amylin, are found in the pancreas.[5,6]

Despite the fact that most peptides and proteins may be turned into an amyloid-like structure under the right conditions,[7] the route leading to fibril formation is still not well understood as it might follow different mechanisms.[4,8] These are natural functions of the protein or peptide sequence but also depend on the sample preparation and fibril growth conditions[9−11] and the use of seeding.[12] This in turn leads to a large variety of fibril morphologies starting from the peptide arrangement within the β-sheets[13−18] to the number and degree of intertwining of protofibrils.[19,20] Nevertheless, in most cases, fibril formation starts by (partial) unfolding followed by misfolding of the peptide/protein monomers, which then aggregate into amorphous oligomers. These oligomers form protofibrils, which associate to form fibrils. Notably, it is now believed that the cyto- and neurotoxic species are the early oligomers and protofibrils, which may act by forming pores in cell membranes and lyse the cell,[21] also observed for amylin.[22−25] This gives an enormous therapeutic potential for the control of amyloid fibril formation.

The study of supramolecular assembly of protofibrils is extremely challenging by both experimental and conventional computational approaches,[26−34] which cannot provide a fine understanding of the entire assembly process. Here, we use coarse-grained (CG) molecular dynamics (MD) simulations to provide a level of resolution between the nanometer range of AFM and EM and atomistic structures. Our aim is, rather than looking at the complete fibril formation process, to study a particular step of the process corresponding to the one studied by AFM, namely, the aggregation of preformed oligomers or protofibril fragments. Thereby, the initial steps of the misfolding and peptide aggregation process are skipped. The use of oligomers as seeds to form end stage fibrils was motivated by recent studies of amylin, showing a significant increase in aggregation time,[10] and from similar studies on the HET-s fibril.[11] The study may thus relate to seeding as it follows the initial stages of interaction between potential seeds.

Amylin is a perfect working case because its assembly process into amyloid fibrils follows all of the above dependencies and extensive structural studies have been performed.[15,35−38] Notably, amylin aggregates are formed by two intertwining protofibrils[39,40] or more depending on the experimental conditions.[39] The growth of amylin fibrils in solution is proposed to occur in two phases; first, the fibrils grow laterally to a given width, after which elongation takes place.[41] This implies that protofibrils are not formed independently in solution but are subunits of the larger growing fibril, which is in agreement with the small number of protofibrils

Received: July 22, 2011
Accepted: September 1, 2011
Published: September 02, 2011

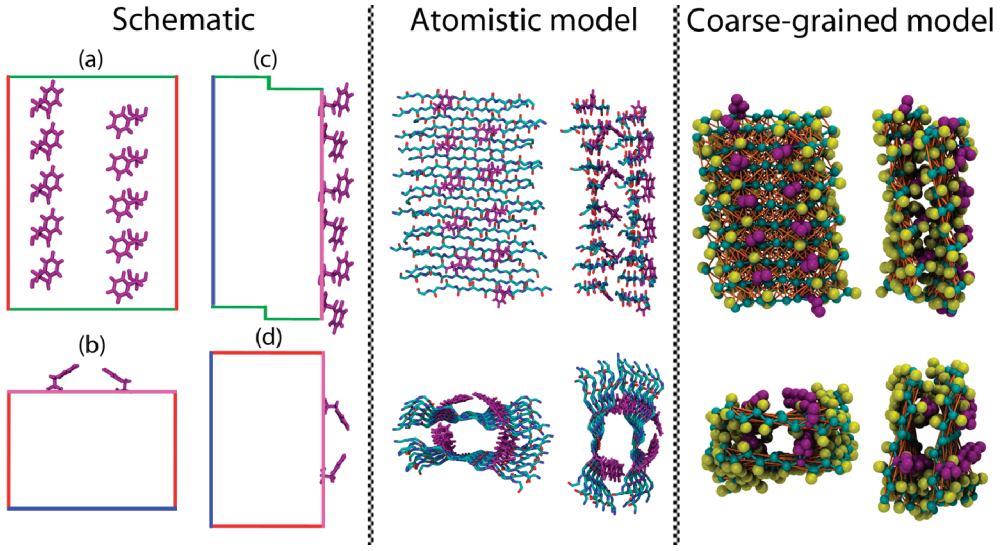

Figure 1. Each prefibrillar oligomer contains 20 decapeptides, 10 in each β-sheet. One face contains the side-chain of Phe23 pointing outward (F-Face), and one does not (nonF-Face). The two edge surfaces formed by the peptide termini are almost identical (referred to as TerA and TerB), as are the elongation end surfaces (ElongA and ElongB), except for the shift caused by the in-register alignment of the peptides. The orientation of the protofibril fragment used, shown in a schematic view (left), an all-atom structure (middle) (only the side-chain of the Phe residue is shown for clarity), and the CG representations (right). The sides in the schematic representation are colored to indicate the orientation, F-Face (purple), nonF-Face (blue), TerA and TerB (red), and ElongA and ElongB (green). (a) Showing the face with the Phe residues pointing outward. (b) Showing one of the elongation ends. (c) Showing the lateral edge. (d) Showing the elongation edge, rotated.

observed.[41] When fibrils are formed on a mica support, protofibrils are more readily observed.[40−42]

In this study, we use the decapeptide hIAPP(20−29) as a model system. It forms fibrils similar to the full length amylin.[12] A CG model compatible with the MARTINI force field for biomolecules[43] and its extension to proteins[44] was used. The model was calibrated based on atomistic (AT) simulations of both NFGAILS (hIAPP(22−28)) and SNNFGAILSS (hIAPP(20−29)) peptides in a protofibril arrangement containing two β-sheets with 18 and 10 peptides each, respectively (see the Supporting Information for details). The initial conformation was taken from the solid-state NMR model with the PDB-ID 2KIB.[15] It is an antiparallel ladder "hetero zipper"; the peptides in a β-sheet are antiparallel, and the sheets are parallel so that the two faces of the protofibril are different (Figure 1). An elastic network, ElNeDyn,[45] was used to preserve the structure of the two β-sheets independently, that is, the sheets have their own network. In the spirit of the ElNeDyn approach, the extent of the network (0.9 nm) and its strength (1000 kJ/mol) were tuned to reproduce the dynamics of the protofibril in the atomistic simulations (see the Supporting Information for detail). The elastic network also preserves the twist of the protofibrils, which was found stable for cross-β structures in solution.[46]

The assembly process was studied by following 27 SNNFGAILSS protofibril fragments placed on a $3 \times 3 \times 3$ grid with randomized orientations and solvated in a box of water (see Figure 2a). The system was simulated for 10 μs* at 300 K. The * indicates that this is an effective time (simulation time multiplied by a factor of 4), accounting for the average speedup of the dynamics in the MARTINI CG force field.[43,47] The assembly process was followed by means of the protofibril burial, defined as the area of the protofibril surface involved in contact with other protofibrils.

The formation of the first contacts in the simulations is relatively fast, as shown in Figure 3a. Within the first μs*, the protein degree of burial already reaches a level close to the final percentage. During the remaining time, the degree of burial slowly grows and reaches a plateau value of 35%. This dual regime is representative of the formation of a rapid encounter complex followed by a slow maximization of the protein−protein interfaces.[48−51] A simple visual inspection (Figure 2b) revealed that the aggregate formed does not resemble mature amyloid fibrils but is rather disordered. However, ordered segments within the assemblies of protofibrils are observed, that is, elongation ends coming together and termini edges associating (Figure 2b). The decomposition of the total burial of the protofibrils segments into the different sides, shown in Figure 1, revealed a slight but significant inequality between the interfaces, suggesting a potential specific trend in the association process (Figure 3b). At 300 K, the elongation ends are the faces of the protofibril fragments engaging the largest part of their surface into contacts. This indicates that these interfaces engage in better or more complete contacts with other protofibril fragments than the other interfaces. This might be due to the smaller size of this interface. It is also notable that the degree of burial measured in percent indicates that none of the interfaces are systematically engaged into complete contacts. Growth of mature fibrils is clearly not observed as fibrils get stuck in disordered intermediates. The presence of only a limited amount of well-ordered interfaces is in line with the work by Wu et al., who reported atomistic simulations of NFGAIL peptides in which only 8% of the oligomers were ordered even though 85% of the peptides were involved in oligomers. They proposed that the rate-limiting step in the formation of well-ordered oligomers is the dissociation of disordered oligomers, to allow for correct reassembly.[18] Here, we did not observe dissociation of the protofibril segments after their first encounter, but a clear reorganization of the fibril's interfaces in the aggregate was revealed by the time evolution of the distribution of the fibril burial (Figure 3c; the detail of each interface is given as Supporting Information). However, it is likely that the observation by Wu et al. also applies

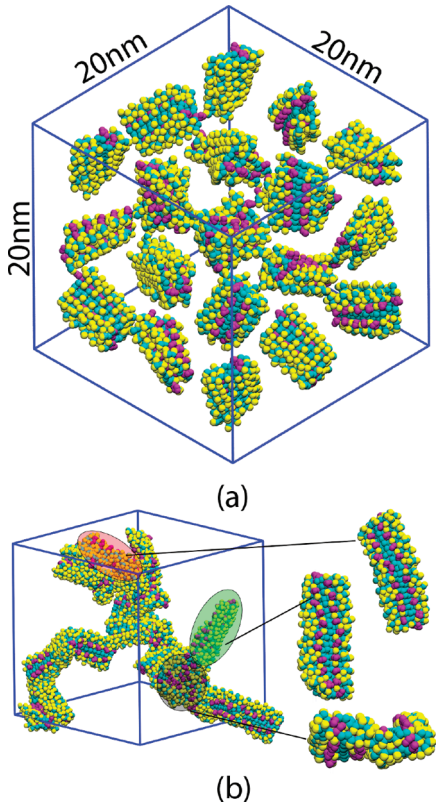

Figure 2. (a) The initial setup of 27 protofibrillar fragments in grid points, with their orientations randomized. (b) The assembly of the protofibrils after 2 μs* at 300 K. Among the disordered aggregates, well-ordered aggregates exist, as highlighted. Two protofibrils have assembled edge-to-edge (marked by black), and two sets of two protofibrillar fragments have assembled in an elongated fashion, marked by red and green, respectively.

to our case, in which we found that 100% of the protofibrils are involved in contacts.

To increase the sampling speed, we performed additional simulations at higher temperatures of 400 and 500 K. These temperatures are significantly higher than those used in laboratory experiments; however, on the time scales studied here, the model's responses to temperature changes are not expected to be as large as those in experimental conditions; higher temperatures may be used to observe trends. The results are also displayed in Figure 3. Compared to the lower-temperature case, the speed of initial contact formation is even faster, and the final degree of burial reaches levels of 41 and 58% at 400 and 500 K, respectively. While the speed up of the initial contact formation with increasing temperature is most likely due to an increase of the diffusion rate, the increase of the overall degree of burial of the protofibril segments results from an optimization of the interfaces. Furthermore, the evolution of the protofibril degree of burial of the different interfaces with the temperature shows that the preferential growth observed at 300 K is abolished as all of the interfaces reach a higher but similar level of burial at high temperatures. Altogether, these observations indicate that the use of high temperatures in the simulations modifies the assembly pathway observed at 300 K and was therefore not pursued.

Next, in order to increase statistics of the early burial events, 10 different sets of randomized orientations were built, and each was simulated for 2 μs* at 300 K. The averages and distributions of the degree of burial of the different interfaces collected over the 27 protofibrils in the last 500 ns* of the 10 $\times$ 2 μs* simulations are shown in Figure 4. One can grossly assume that the termini edges, F-Face, and nonF-Face degrees of burial follow a normal distribution (occasionally slightly asymmetric) of around 15, 25, and 35%, respectively. Only a very limited proportion showed more than 50% burial. The case of the elongation ends is quite different. They also possess a large proportion of protofibrils with burial degrees lower than 50%, but in contrast to the other interfaces, they have a significant amount of cases where the burial degree is above 65%. This last case could be grossly described by a bimodal distribution. The burial degree of the protofibrils engaged in the end-to-end contacts shown in Figure 4 are between 70 and 80%, which is close to the level of burial expected for a complete assembly of these interfaces (80% is found for an ideal interface; see the Supporting Information).

In summary, all of the interfaces have a certain degree of involvement in contacts, on average, 25% of burial, which could be assimilated with random encounters occurring during the early stage of the assembly. The elongation ends engage a significant amount of more complete contacts. Altogether, this suggests a preferential growth by elongation at the stage of the amyloid fibril formation studied here. Note that this preferential growth is lost with an increase of temperature, as mentioned earlier. Although this preferential elongation growth might be contradictory to experiments in which a lateral growth of the oligomers occurred prior to elongation, the size of the oligomers observed in the experiments indicates that we are not in the same structural regime. The oligomers or seeds used in this work are much shorter, $\sim$4.5 versus $\sim$23 nm in the experiments,[41] and therefore should first elongate.

To put our results into perspective, it is important to reflect on some of the limitations underlying our model. First, it is important to stress that the time scales explored in the simulations restrict our analysis of the fibril formation to the early events of the association of protofibrils fragments. The formation of amyloid fibrils in vitro may take days, which is orders of magnitude longer than what is currently within reach of computer simulations, even using CG models. We therefore may only report on early events of the amyloid formation. Similarly, the overall system size used, although significantly larger than current standards, and the size of the protofibril fragments might affect the growth mechanism observed. Second, in the MARTINI coarse-grained model, the secondary structure of a protein is constrained. There is no possibility to observe a rearrangement of the secondary structure. This is a fair approximation because the protofibril fragments are not expected to change structure. However, the underlying reason for the use of constrained protein secondary structure is the lack of directionality of the H-bonds in the model, which prevents a backbone bead from having a preferential interaction with another backbone bead in a secondary structure element rather than with the surrounding solvent. Instead, the interactions are guided, and the relative strength of the backbone bead interactions with its surroundings is reduced when it is involved in a secondary structure.[44] This particular way to treat the backbone−backbone interactions might have impaired the interactions between the protofibrils and especially when elongation ends were involved. In this way, the elongation-like growth described above might actually be underestimated. Third, as a consequence of the secondary structure dependency of the backbone, the addition of free peptides in the simulation box is not possible, although their

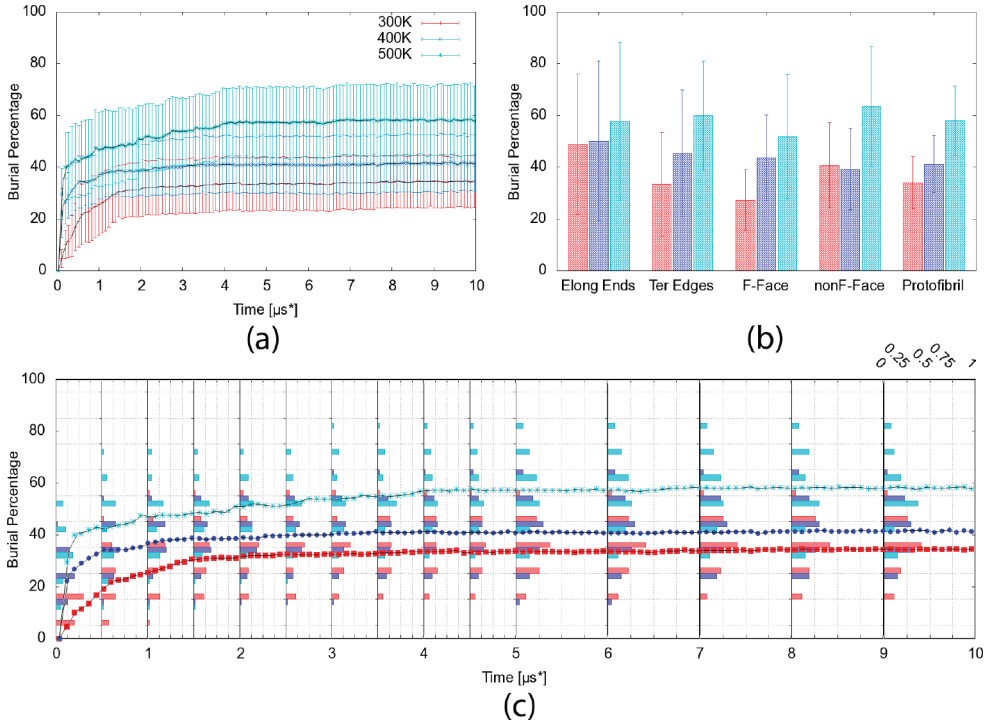

Figure 3. (a) The averaged burial degree calculated for the 27 protofibrils as a function of time at 300, 400, and 500 K, including standard deviations (shown in red, blue, and cyan, respectively). (b) The averaged burial degree (in the 5−10 μs time period) of each surface of the protofibrils at the three temperatures, with standard deviations. (c) The distribution of burial degree for the protofibrils as a function of time. The histograms have a bin width of 10% burial; the upper scale is the number of protofibrils (normalized). The data shown in (a) is also included in panel (c).

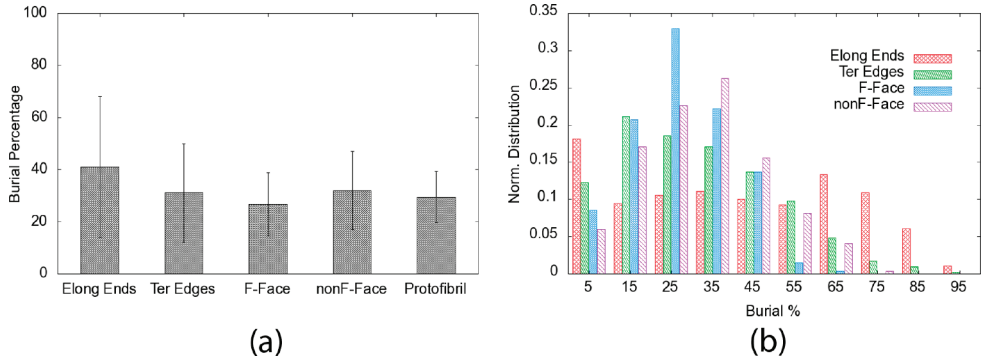

Figure 4. (a) The degree of burial for the complete protofibril and the different surfaces averaged over the 27 protofibrils and the 10 simulations and (b) the distribution of the burial percentage for these surfaces. In this decomposition, the two elongation ends and the two termini edges are grouped together (see Figure 1 legend). Graphs showing the burial degree of each protofibril surface of every fibril for each of the 10 simulations are available in the Supporting Information, along with figures showing the bead selection for the surface definitions.

involvement in the fibril growth might be determinant. Other CG models allow studying of peptides individually.[28,29] Fourth, a direct consequence of the previous point is that the current simulations do not allow an estimation of the thermodynamic and kinetic contributions to the control of the growth mechanism, although it is an important aspect.[52] Note that current developments of our CG force field are aiming at removing the secondary structure dependency of the backbone by restoring the directionality of the interactions. Finally, there are some indications that the MARTINI force field might overstabilize protein−protein interactions in an aqueous environment. This might be reflected by the relatively quick formation of contacts. The relative strength and population of the interfaces observed through the large statistics should of course not be affected.

We have described the formation of aggregates from small prefibrillar oligomers using CG MD simulations. Notably, the results show that the initial aggregation is relatively fast and that a slower reorganization stage leads to higher-ordered amyloid fibrillar structures. We also found that the model follows a preferential growth mechanism favoring the elongation of the protofibrils used. The model also experienced a change of growth mechanism when changing the growth conditions, which were mimicked here by a change in temperature. This is in line with experimental evidence. Although our results are still limited to the computationally accessible system sizes and time scales, they

prove the great potential of this type of approach in participating in the elucidation of the amyloid fibril formation mechanism. The continuous improvement of the models will certainly provide valuable mechanistic information.

COMPUTATIONAL DETAILS

Explicit solvent all-atom MD simulations were performed with the AMBER03 force field[53] in NAMD 2.7[54] using the ssNMR pdb structure of the NFGAILS as a starting structure and with remodeling of the full SNNFGAILSS decapeptide, preceded by minimization, heating, and equilibration, using the protocol described previously.[55] The peptides in the AT simulations were capped, and likewise, the termini in the CG simulations were uncharged. The structures were mapped in the CG MARTINI model[43,44] using tools available on the MARTINI Web site, www.cgmartini.nl. The ElNeDyn approach was used to retain the overall structure of the protofibril.[45] The CG simulations have been performed in Gromacs 4.0.7.[56] The orientation of each of the 27 protofibrils in the system was randomized, and each system was simulated using a different seed for generation of initial velocities. The box size and the grid were chosen so that at least 1.5 nm separated the protofibrils. To quantify the involvement of a particular side of the protofibril into the aggregation, its degree of burial (or buried solvent accessibility surface area, SASA) was estimated relative to the free protofibril according to

$$\text{Degree of burial} = 100\% \times (1 - [\text{SASA(X)}/\text{SASA}(\text{X}_{\text{ref}})])$$

where $\text{SASA}(\text{X}_{\text{ref}})$ is the calculated SASA of the X surface without considering its contacts with other protofibrils and SASA(X) is the SASA of the same X surface taking into account the contacts with the other protofibrils. The SASA calculations were done in VMD.[57] The radii of the CG beads were scaled to their correct size, and the radius of the probe in the SASA calculations on the CG simulations had a radius of 0.264 nm, corresponding to the size of the CG bead. The atoms used to define a surface are shown in the Supporting Information.

ASSOCIATED CONTENT

Supporting Information. A comparison of the dynamics between the AT and CG simulations of the NFGAILS and SNNFGAILSS protofibril fragments, tuning of ElNeDyn parameters, solvent accessible surface area definitions, and details about the burial of each fibril in each simulation. This material is available free of charge via the Internet at http://pubs.acs.org. The parameter files are available on the MARTINI Web site: www.cgmartini.nl.

AUTHOR INFORMATION

Corresponding Author

*Phone: +4589423953. Fax: +4586196199. E-mail: birgit@chem.au.dk.

ACKNOWLEDGMENT

J.S., K.K.S., and B.S. acknowledge funding from The Danish Council for Independent Research (Natural Sciences), the Lundbeck and Carlsberg Foundations, the centers for Insoluble Protein Structures (inSPIN) and Theory in Natural Sciences (CTN) at Aarhus University, as well as computer allocations from the HPC-EUROPA2 project (project number: 228398) with the support of the European Commission (Capacities Area - Research Infrastructures) and the Danish Center for Scientific Computing, specifically the Center for Scientific Computing Aarhus. X.P. and S.-J.M. acknowledge funding from The Netherlands Organisation for Scientific Research (NWO).

REFERENCES

(1) Eanes, E. D.; Glenner, G. G. X-Ray Diffraction Studies on Amyloid Filaments. *J. Histochem. Cytochem.* **1968**, *16*, 673–677.

(2) Sunde, M.; Serpell, L.; Bartlam, M.; Fraser, P. E.; Pepys, M. B.; Blake, C. C. F. Common Core Structure of Amyloid Fibrils by Synchrotron X-Ray Diffraction. *J. Mol. Biol.* **1997**, *273*, 729–739.

(3) Sacchettini, J. C.; Kelly, J. W. Therapeutic Strategies of Human Amyloid Diseases. *Nat. Rev. Drug Discovery* **2002**, *1*, 267–275.

(4) Chiti, F.; Dobson, C. M. Protein Misfolding, Functional Amyloid, and Human Disease. *Annu. Rev. Biochem.* **2006**, *75*, 333–366.

(5) Cooper, G. J.; Willis, A. C.; Clark, A.; Turner, R. C.; Sim, R. B.; Reid, K. B. Purification and Characterization of a Peptide from Amyloid-Rich Pancreases of Type 2 Diabetic Patients. *Proc. Natl. Acad. Sci. U.S.A.* **1987**, *84*, 8628–8632.

(6) Westermark, P.; Wernstedt, C.; Wilander, E.; Hayden, D. W.; O'Brien, T. D.; Johnson, K. H. Amyloid Fibrils in Human Insulinoma and Islets of Langerhans of the Diabetic Cat are Derived from a Neuropeptide-Like Protein also Present in Normal Islet Cells. *Proc. Natl. Acad. Sci. U.S.A.* **1987**, *84*, 3881–3885.

(7) Chiti, F.; Webster, P.; Taddei, N.; Clark, A.; Stefani, M.; Ramponi, G.; Dobson, C. M. Designing Conditions for in Vitro Formation of Amyloid Protofilaments and Fibrils. *Proc. Natl. Acad. Sci. U.S.A.* **1999**, *96*, 3590–3594.

(8) Kumar, S.; Udgaonkar, J. B. Mechanisms of Amyloid Fibril Formation by Proteins. *Curr. Sci.* **2010**, *98*, 639–656.

(9) Pedersen, J. S.; Dikov, D.; Flink, J. L.; Hjuler, H. A.; Christiansen, G.; Otzen, D. E. The Changing Face of Glucagon Fibrillation: Structural Polymorphism and Conformational Imprinting. *J. Mol. Biol.* **2006**, *355*, 501–523.

(10) Kayed, R.; Bernhagen, J.; Greenfield, N.; Sweimeh, K.; Brunner, H.; Voelter, W.; Kapurniotu, A. Conformational Transitions of Islet Amyloid Polypeptide (IAPP) in Amyloid Formation *in Vitro*. *J. Mol. Biol.* **1999**, *287*, 781–796.

(11) Mizuno, N.; Baxa, U.; Steven, A. C. Structural Dependence of HET-s Amyloid Fibril Infectivity Assessed by Cryoelectron Microscopy. *Proc. Natl. Acad. Sci. U.S.A.* **2011**, *108*, 3252–3257.

(12) Madine, J.; Jack, E.; Stockley, P. G.; Radford, S. E.; Serpell, L. C.; Middleton, D. A. Structural Insights into the Polymorphism of Amyloid-Like Fibrils Formed by Region 20−29 of Amylin Revealed by Solid-State NMR and X-Ray Fiber Diffraction. *J. Am. Chem. Soc.* **2008**, *130*, 14990–15001.

(13) Ashburn, T. T.; Auger, M.; Lansbury, P. T. The Structural Basis of Pancreatic Amyloid Formation: Isotope-Edited Spectroscopy in the Solid-State. *J. Am. Chem. Soc.* **1992**, *114*, 790–791.

(14) Griffiths, J. M.; Ashburn, T. T.; Auger, M.; Costa, P. R.; Griffin, R. G.; Lansbury, P. T. Rotational Resonance Solid-State NMR Elucidates a Structural Model of Pancreatic Amyloid. *J. Am. Chem. Soc.* **1995**, *117*, 3539–3546.

(15) Nielsen, J. T.; Bjerring, M.; Jeppesen, M. D.; Pedersen, R. O.; Pedersen, J. M.; Hein, K. L.; Vosegaard, T.; Skrydstrup, T.; Otzen, D. E.; Nielsen, N. C. Unique Identification of Supramolecular Structures in Amyloid Fibrils by Solid-State NMR Spectroscopy. *Angew. Chem., Int. Ed.* **2009**, *48*, 2118–2121.

(16) Zanuy, D.; Ma, B. Y.; Nussinov, R. Short Peptide Amyloid Organization: Stabilities and Conformations of the Islet Amyloid Peptide NFGAIL. *Biophys. J.* **2003**, *84*, 1884–1894.

(17) Wu, C.; Lei, H. X.; Duan, Y. The Role of Phe in the Formation of Well-Ordered Oligomers of Amyloidogenic Hexapeptide (NFGAIL) Observed in Molecular Dynamics Simulations with Explicit Solvent. *Biophys. J.* **2005**, *88*, 2897–2906.

(18) Wu, C.; Lei, H.; Duan, Y. Elongation of Ordered Peptide Aggregate of an Amyloidogenic Hexapeptide NFGAIL Observed in Molecular Dynamics Simulations with Explicit Solvent. *J. Am. Chem. Soc.* **2005**, *127*, 13530–13537.

(19) Dong, M.; Hovgaard, M. B.; Xu, S.; Otzen, D. E.; Besenbacher, F. AFM Study of Glucagon Fibrillation Via Oligomeric Structures Resulting in Interwoven Fibrils. *Nanotechnology* **2006**, *17*, 4003–4009.

(20) De Jong, K. L.; Incledon, B.; Yip, C. M.; DeFelippis, M. R. Amyloid Fibrils of Glucagon Characterized by High-Resolution Atomic Force Microscopy. *Biophys. J.* **2006**, *91*, 1905–1914.

(21) Lashuel, H. A.; Lansbury, P. T., Jr. Are Amyloid Diseases Caused by Protein Aggregates that Mimic Bacterial Pore-Forming Toxins? *Q Rev. Biophys.* **2006**, *39*, 167–201.

(22) Lorenzo, A.; Razzaboni, B.; Weir, G. C.; Yankner, B. A. Pancreatic Islet Cell Toxicity of Amylin Associated with Type-2 Diabetes Mellitus. *Nature* **1994**, *368*, 756–760.

(23) Mirzabekov, T. A.; Lin, M.; Kagan, B. L. Pore Formation by the Cytotoxic Islet Amyloid Peptide Amylin. *J. Biol. Chem.* **1996**, *271*, 1988–1992.

(24) Sparr, E.; Engel, M. F. M.; Sakharov, D. V.; Sprong, M.; Jacobs, J.; de Kruijff, B.; Höppener, J. W. M.; Antoinette Killian, J. Islet Amyloid Polypeptide-Induced Membrane Leakage Involves Uptake of Lipids by Forming Amyloid Fibers. *FEBS Lett.* **2004**, *577*, 117–120.

(25) Last, N. B.; Rhoades, E.; Miranker, A. D. Islet Amyloid Polypeptide Demonstrates a Persistent Capacity to Disrupt Membrane Integrity. *Proc. Natl. Acad. Sci. U.S.A.* **2011**, *108*, 9460–9465.

(26) Wu, C.; Shea, J. Coarse-Grained Models for Protein Aggregation. *Curr. Opin. Struct. Biol.* **2011**, *21*, 209–220.

(27) Masman, M. F.; Eisel, U. L. M.; Csizmadia, I. G.; Penke, B.; Enriz, R. D.; Marrink, S. J.; Luiten, P. G. M. *In Silico* Study of Full-Length Amyloid β 1−42 Tri- and Penta-Oligomers in Solution. *J. Phys. Chem. B* **2009**, *113*, 11710–11719.

(28) Magno, A.; Caflisch, A.; Pellarin, R. Crowding Effects on Amyloid Aggregation Kinetics. *J. Phys. Chem. Lett.* **2010**, *1*, 3027–3032.

(29) Nasica-Labouze, J.; Meli, M.; Derreumaux, P.; Colombo, G.; Mousseau, N. A Multiscale Approach to Characterize the Early Aggregation Steps of the Amyloid-Forming Peptide GNNQQNY from the Yeast Prion Sup-35. *PLoS Comput. Biol.* **2011**, *7*, e1002051.

(30) Pellarin, R.; Guarnera, E.; Caflisch, A. Pathways and Intermediates of Amyloid Fibril Formation. *J. Mol. Biol.* **2007**, *374*, 917–924.

(31) Wagoner, V. A.; Cheon, M.; Chang, I.; Hall, C. K. Computer Simulation Study of Amyloid Fibril Formation by Palindromic Sequences in Prion Peptides. *Proteins* **2011**, *79*, 2132–45.

(32) Lee, C. F.; Loken, J.; Jean, L.; Vaux, D. J. Elongation Dynamics of Amyloid Fibrils: A Rugged Energy Landscape Picture. *Phys. Rev. E* **2009**, *80*, 041906.

(33) Wolf, M. G.; van Gestel, J.; de Leeuw, S. W. Modeling Amyloid Fibril Formation A Free-Energy Approach. *Methods Mol. Biol.* **2008**, *474*, 153–179.

(34) Shaytan, A. K.; Khokhlov, A. R.; Khalatur, P. G. Large-Scale Atomistic Simulation of a Nanosized Fibril Formed by Thiophene-Peptide "Molecular Chimeras". *Soft Matter* **2010**, *6*, 1453–1461.

(35) Kajava, A. V.; Aebi, U.; Steven, A. C. The Parallel Superpleated β-Structure as a Model for Amyloid Fibrils of Human Amylin. *J. Mol. Biol.* **2005**, *348*, 247–252.

(36) Luca, S.; Yau, W.; Leapman, R.; Tycko, R. Peptide Conformation and Supramolecular Organization in Amylin Fibrils: Constraints from Solid-State NMR. *Biochemistry* **2007**, *46*, 13505–13522.

(37) Wiltzius, J. J. W.; Sievers, S. A.; Sawaya, M. R.; Cascio, D.; Popov, D.; Riekel, C.; Eisenberg, D. Atomic Structure of the Cross-β Spine of Islet Amyloid Polypeptide (Amylin). *Protein Sci.* **2008**, *17*, 1467–1474.

(38) Tenidis, K.; Waldner, M.; Bernhagen, J.; Fischle, W.; Bergmann, M.; Weber, M.; Merkle, M. L.; Voelter, W.; Brunner, H.; Kapurniotu, A. Identification of a Penta- and Hexapeptide of Islet Amyloid Polypeptide (IAPP) with Amyloidogenic and Cytotoxic Properties. *J. Mol. Biol.* **2000**, *295*, 1055–1071.

(39) Goldsbury, C. S.; Cooper, G. J. S.; Goldie, K. N.; Muller, S. A.; Saafi, E. L.; Gruijters, W. T. M.; Misur, M. P. Polymorphic Fibrillar Assembly of Human Amylin. *J. Struct. Biol.* **1997**, *119*, 17–27.

(40) Goldsbury, C.; Kistler, J.; Aebi, U.; Arvinte, T.; Cooper, G. J. S. Watching Amyloid Fibrils Grow by Time-Lapse Atomic Force Microscopy. *J. Mol. Biol.* **1999**, *285*, 33–39.

(41) Green, J. D.; Goldsbury, C.; Kistler, J.; Cooper, G. J. S.; Aebi, U. Human Amylin Oligomer Growth and Fibril Elongation Define Two Distinct Phases in Amyloid Formation. *J. Biol. Chem.* **2004**, *279*, 12206–12212.

(42) Cho, W.; Jena, B. P.; Jeremic, A. M. Nano-Scale Imaging and Dynamics of Amylin-Membrane Interactions and Its Implication in Type II Diabetes Mellitus. In *Methods in Cell Biology*; Jena, B. P., Ed.; Academic Press: New York, 2008; Vol. 90,Chapter 13 , pp 267−286.

(43) Marrink, S. J.; Risselada, H. J.; Yefimov, S.; Tieleman, D. P.; de Vries, A. H. The MARTINI Force Field: Coarse Grained Model for Biomolecular Simulations. *J. Phys. Chem. B* **2007**, *111*, 7812–7824.

(44) Monticelli, L.; Kandasamy, S. K.; Periole, X.; Larson, R. G.; Tieleman, D. P.; Marrink, S. J. The MARTINI Coarse-Grained Force Field: Extension to Proteins. *J. Chem. Theory Comput.* **2008**, *4*, 819–834.

(45) Periole, X.; Cavalli, M.; Marrink, S. J.; Ceruso, M. A. Combining an Elastic Network with a Coarse-Grained Molecular Force Field: Structure, Dynamics, and Intermolecular Recognition. *J. Chem. Theory Comput.* **2009**, *5*, 2531–2543.

(46) Periole, X.; Rampioni, A.; Vendruscolo, M.; Mark, A. E. Factors that Affect the Degree of Twist in β-Sheet Structures: A Molecular Dynamics Simulation Study of a Cross-β Filament of the GNNQQNY Peptide. *J. Phys. Chem. B* **2009**, *113*, 1728–1737.

(47) Marrink, S. J.; de Vries, A. H.; Mark, A. E. Coarse Grained Model for Semiquantitative Lipid Simulations. *J. Phys. Chem. B* **2004**, *108*, 750–760.

(48) Gabdoulline, R. R.; Wade, R. C. Biomolecular Diffusional Association. *Curr. Opin. Struct. Biol.* **2002**, *12*, 204–213.

(49) Tang, C.; Iwahara, J.; Clore, G. M. Visualization of Transient Encounter Complexes in Protein-Protein Association. *Nature* **2006**, *444*, 383–386.

(50) Grunberg, R.; Leckner, J.; Nilges, M. Complementarity of Structure Ensembles in Protein-Protein Binding. *Structure* **2004**, *12*, 2125–2136.

(51) Periole, X.; Huber, T.; Marrink, S. J.; Sakmar, T. P. G Protein-Coupled Receptors Self-Assemble in Dynamics Simulations of Model Bilayers. *J. Am. Chem. Soc.* **2007**, *129*, 10126–10132.

(52) Pellarin, R.; Schuetz, P.; Guarnera, E.; Caflisch, A. Amyloid Fibril Polymorphism is Under Kinetic Control. *J. Am. Chem. Soc.* **2010**, *132*, 14960–14970.

(53) Duan, Y.; Wu, C.; Chowdhury, S.; Lee, M. C.; Xiong, G.; Zhang, W.; Yang, R.; Cieplak, P.; Luo, R.; Lee, T.; et al. A Point-Charge Force Field for Molecular Mechanics Simulations of Proteins Based on Condensed-Phase Quantum Mechanical Calculations. *J. Comput. Chem.* **2003**, *24*, 1999–2012.

(54) Phillips, J. C.; Braun, R.; Wang, W.; Gumbart, J.; Tajkhorshid, E.; Villa, E.; Chipot, C.; Skeel, R. D.; Kalé, L.; Schulten, K. Scalable Molecular Dynamics with NAMD. *J. Comput. Chem.* **2005**, *26*, 1781–1802.

(55) Sørensen, J.; Hamelberg, D.; Schiøtt, B.; McCammon, J. A. Comparative MD Analysis of the Stability of Transthyretin Providing Insight into the Fibrillation Mechanism. *Biopolymers* **2007**, *86*, 73–82.

(56) Hess, B.; Kutzner, C.; van, d. S.; Lindahl, E. GROMACS 4: Algorithms for Highly Efficient, Load-Balanced, and Scalable Molecular Simulation. *J. Chem. Theory Comput.* **2008**, *4*, 435–447.

(57) Humphrey, W.; Dalke, A.; Schulten, K. VMD: Visual Molecular Dynamics. *J. Mol. Graphics Model.* **1996**, *14*, 33–38.